University of Reading

Intact myocardial preparations reveal intrinsic transmural heterogeneity in cardiac mechanics

Article

Accepted Version

It is advisable to refer to the publisher's version if you intend to cite from the work. See Guidance on citing.
Published version at: http://dx.doi.org/10.1016/j.yjmcc.2020.03.007
To link to this article DOI: http://dx.doi.org/10.1016/j.yjmcc.2020.03.007

www.reading.ac.uk/centaur

CentAUR

Central Archive at the University of Reading

Reading's research outputs online
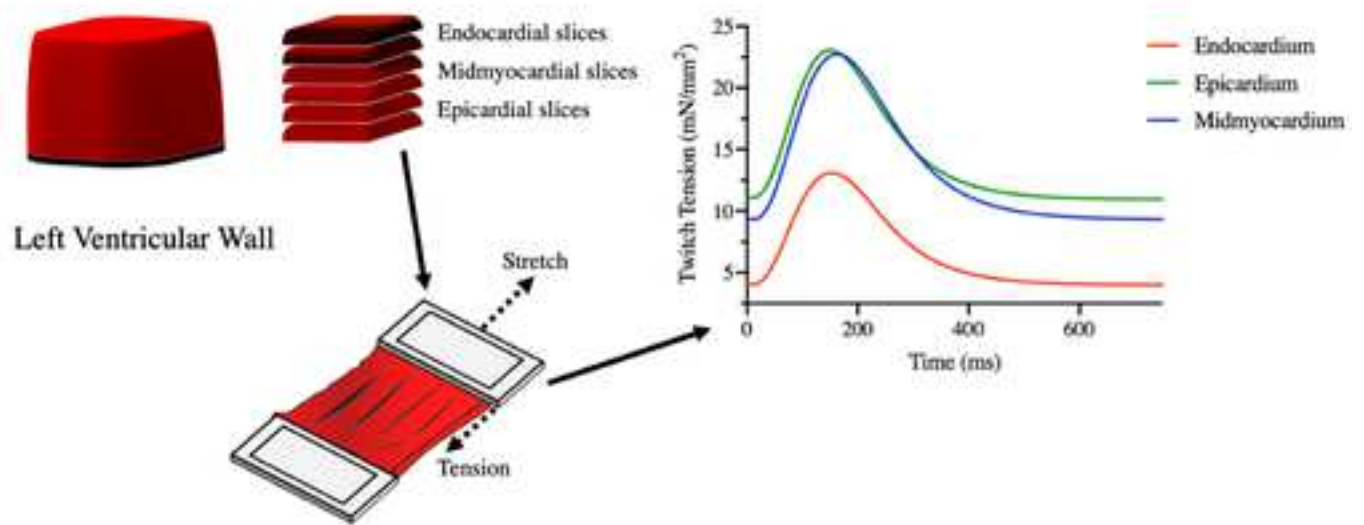
Graphical Abstract

Endocardial slices
Midmyocardial slices
Epicardial slices

Left Ventricular Wall

Stretch

Tension

Twitch Tension (mN/mm²)

Time (ms)

Endocardium
Epicardium
Midmyocardium

Highlights

- The myocardial slice preparation is an intact cardiac model allowing the study of transmural properties.
- Mechanical behaviour is cardiac layer dependent.
- Structural differences in cardiomyocyte density, orientation, and aspect ratio may contribute to these findings.

1 Intact myocardial preparations reveal intrinsic transmural hetero-
2 geneity in cardiac mechanics
3

4 Authors List

5 Fotios G Pitoulis[1], Waseem Hasan[1], Maria Papadaki[2], Nicolas G Clavere[3], Filippo
6 Perbellini[1, 4], Sian E Harding[1], Jonathan A Kirk[2], Samuel Y Boateng[3], Pieter P de
7 Tombe[1, 2], Cesare M Terracciano[1]
8

9 1: National Heart and Lung Institute, Imperial College London, UK
10 2: Department of Cell and Molecular Physiology, Loyola University Chicago, USA
11 3: School of Biological Sciences, University of Reading, UK
12 4: Institute for Molecular and Translational Therapeutic Strategies, Hannover Medical School, DE
13

14 Abstract

15 Determining transmural mechanical properties in the heart provides a foundation to
16 understand physiological and pathophysiological cardiac mechanics. Although work
17 on mechanical characterisation has begun in isolated cells and permeabilised sam-
18 ples, the mechanical profile of living individual cardiac layers has not been exam-
19 ined. Myocardial slices are 300 μm-thin sections of heart tissue with preserved cellu-
20 lar stoichiometry, extracellular matrix, and structural architecture. This allows for
21 cardiac mechanics assays in the context of an intact *in vitro* organotypic preparation.
22 In slices obtained from the subendocardium, midmyocardium and subepicardium of
23 rats, a distinct pattern in transmural contractility is found that is different from that
24 observed in other models. Slices from the epicardium and midmyocardium had a
25 higher active tension and passive tension than the endocardium upon stretch. Differ-
26 ences in total myocyte area coverage, and aspect ratio between layers underlined the
27 functional readouts, while no differences were found in total sarcomeric protein and
28 phosphoprotein between layers. Such intrinsic heterogeneity may orchestrate the
29 normal pumping of the heart in the presence of transmural strain and sarcomere
30 length gradients in the *in vivo* heart.
31

32 Graphical Abstract
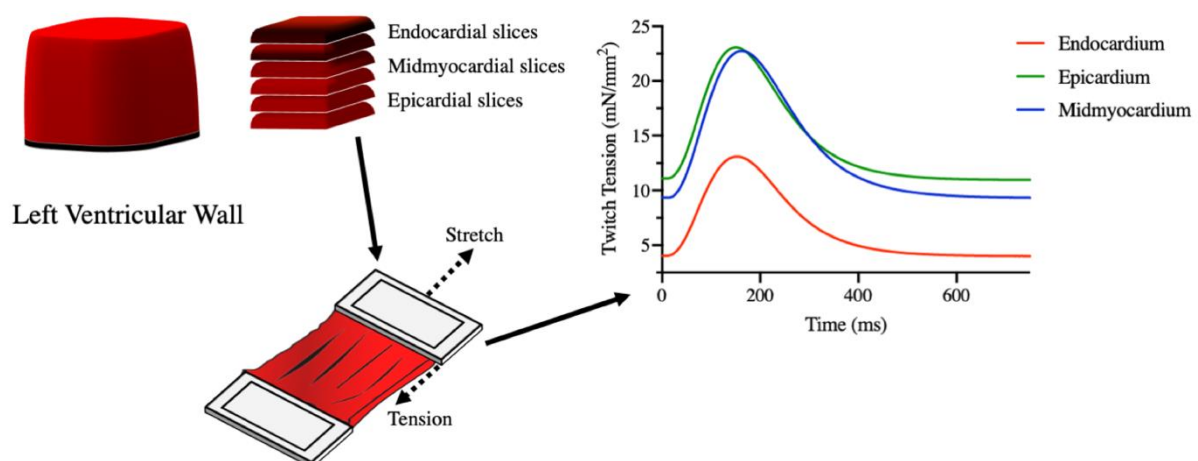
33

Highlights

- The myocardial slice preparation is an intact cardiac model allowing the study of transmural properties.
- Mechanical behaviour is cardiac layer dependent.
- Structural differences in cardiomyocyte density, orientation, and aspect ratio may contribute to these findings.

Keywords

- Transmurality
- Contractility
- Cardiac Mechanics
- Intact Tissue
- Sarcomeric Apparatus
- Extracellular Matrix

1. Introduction

The ventricular myocardium is increasingly recognized as a structure with regional variation. Although differences in electrical properties across the heart wall have been the subject of multiple studies, descriptions of transmural mechanical properties are marred by a paucity of data[1][2].

Determining mechanical behaviour across the heart wall is important as transmural differences in contractility can impact cardiac stroke volume, and changes in transmurality have been observed in human heart failure[2].

However, data on transmural mechanical behavior has been conflicting. Ambiguity remains with respect to whether the endocardium has a higher passive tension (i.e. is stiffer)[3][4] and active tension[3] than the epicardium or not[2][5][6]. Additionally, studies have been limited to isolated cardiomyocytes and permeabilised preparations. Such cardiac models provide insight into the cellular and subcellular basis of transmurality but are restricted in their ability to capture the properties of the *in-situ* myocardium. Isolated cardiomyocytes assess single cells independent of the effect of intercalated discs, extracellular matrix (ECM), multi- & hetero-cellularity in regulating contraction[7], and the transmural variation of these. Likewise, in permeabilised samples, sarcolemmal components and the ECM - both known to affect contractility - are disrupted. Therefore, whether transmural differences observed in these models translate to intact living tissue remains unanswered.

Myocardial slices are a cardiac model of intermediate complexity serving as a bridge between isolated cells and whole heart studies. Slices are 300 μm-thin living organotypic preparations with native cellular architecture, cell-cell/cell-ECM interactions, and preserved metabolic, electric, and mechanical properties[7]. Thus, slices are a novel intact physiological model on which to evaluate cardiac behavior. The slice model permits force vectors to be examined across a 2D plane, enabling mechanical insights comparable to those conducted on isolated cells and permeabilised preparations. Transmural cardiac mechanics were assessed in rat slices and the underlying structural, and sarcomeric differences explored.

2. Methods

2.1. Myocardial Slice Preparation

Myocardial slices were generated as described in [7]. Briefly, slices were prepared from the left ventricles of 11-15-week-old Sprague-Dawley rats (350-470 g) using a high-precision vibratome. Slices were generated in sequence, from endocardium to epicardium. Most ventricles yielded six slices. The earliest slice of 300 μm thickness, after removal of trabeculae carneae, was defined as the first slice. The 1st and 2nd slices were classified as subendocardial myocardium, the 3rd and 4th slice as midmyocardium, and the 5th and 6th slices as subepicardial myocardium. For clarity, these will be referred to as endocardium, midmyocardium and epicardium.

2.2. Laser Diffraction Experiments

The % stretch-sarcomere length relationship was determined using laser diffraction. A high-powered laser was vertically directed on slices, which were progressively stretched, and the diffraction profiles processed in real-time (ImageJ, NIH, USA).

2.3. Contractility Measurements

Contractility was assessed by mounting the slice on an isometric strain gauge (F30 Harvard Apparatus, UK), using custom 3D-printed holders glued on the slice. As myofiber direction rotates across the ventricular wall, holders were always attached perpendicular to main myofiber axis. All slices were stimulated at 1Hz.

2.4. Sarcomeric Protein Content and Phosphorylation Status

Myofilament fractions were generated as previously described[8] from endo-, mid-, and epicardial slices. Total sarcomeric content and phosphoprotein status were quantified using Sypro Ruby and ProQ Diamond stain respectively.

2.5. Immunohistochemistry and Picrosirius Red Staining

Cardiac slices were fixed and stained for caveolin-3, cardiac troponin T, and vimentin, and visualized under confocal microscopy within 1 day of staining. For collagen content hearts were cryosectioned, fixed, stained with Picrosirius red, and visualized under brightfield microscopy.

2.6. Data Analysis

Contractility measurements were analysed using pClamp software (Molecular Devices, USA). Confocal and bright field images, as well as gels were analysed in ImageJ.

2.7. Statistical Analysis

Data sets from each layer were analysed for statistical significance using ANCOVA and one-way ANOVA with Tukey's post-hoc test in Prism 8 (GraphPad, USA). $P < 0.05$ was considered statistically significant.
A detailed description of the methodology is available in the online supplement.

3. Results and Discussion

Cardiac layers have been suggested to operate at different sarcomere lengths (SL) *in vivo*[3][9]. We identified the relationship between % stretch from slack length and SL change (Fig. 1A) using laser diffraction. This allowed control of SL, so that intrinsic differences of each cardiac layers to the same strain could be delineated.

As force production is a function of external Ca^{2+} concentration ($[Ca^{2+}]o$), different force sensitivity to $[Ca^{2+}]o$ would mask intrinsic contractile differences. To account for this, we conducted a series of force-$[Ca^{2+}]o$ experiments with slices stretched to 2.1µm SL (Fig. 1B). Ca^{2+} sensitivity, defined as the $[Ca^{2+}]o$ at which half-maximum force is generated (EC_{50}), was not significantly different between layers (Fig. 1C-Top). It is worth noting that this EC_{50} is a different parameter to the one reported in permeabilised preparations, which describes the response of intracellular components to Ca^{2+}. Permeabilised human endocardial preparations for example, exhibit greater Ca^{2+} sensitivity than the epicardium [2]. In contrast, our data suggests that the Ca^{2+} sensitivity of the intact tissue is homogeneous across the wall. Moreover, the Hill slope, which measures the steepness of the force-$[Ca^{2+}]o$ curve, was not different between layers, further supporting a uniform contractile response to Ca^{2+} (Fig. 1C-Bottom). These experiments yielded a known Ca^{2+} concentration ($EC_{50} = 10^{-2.54}$ M) at which the mechanical properties of the heart could be reliably assessed while controlling for $[Ca^{2+}]o$.

To determine contractile profiles across the wall, Frank-Starling experiments were performed at a range of SLs (2.00–2.40 µm). The midmyocardium produced a significantly higher active tension than the endocardium at SLs 2.20-2.40 µm ($p<0.05$ and $p<0.01$). Higher isometric force and power output has similarly been reported in permeabilised midmyocardium [2]. The epicardium also trended towards higher force development compared to the endocardium (Fig. 1D, $p<0.05$ at SL of 2.35 µm). Contrasting data exists regarding active tension between these latter two layers and results appear to be species-dependent; in ferrets, the endocardium is reported to have a higher maximum active tension than the epicardium[3] whereas in pigs[6] and, more comparably, in rats no differences are described[3]. To quantify the ability of each layer to increase its force output upon stretch, a linear regression was fit to the active tension-SL relationship (Fig. 1D). The slope of this was significantly higher in the epicardium compared to endocardium (Fig. 1E, $p<0.05$), suggesting greater contractile output per µm of stretch. When visualized under light microscopy, slices from the endocardium appear patchier and with recurring gaps between myofibers compared to other layers. Thus, we hypothesized that differences in the cellular composition and tissue architecture may exist and play a role in shaping the observed transmural mechanical heterogeneity.
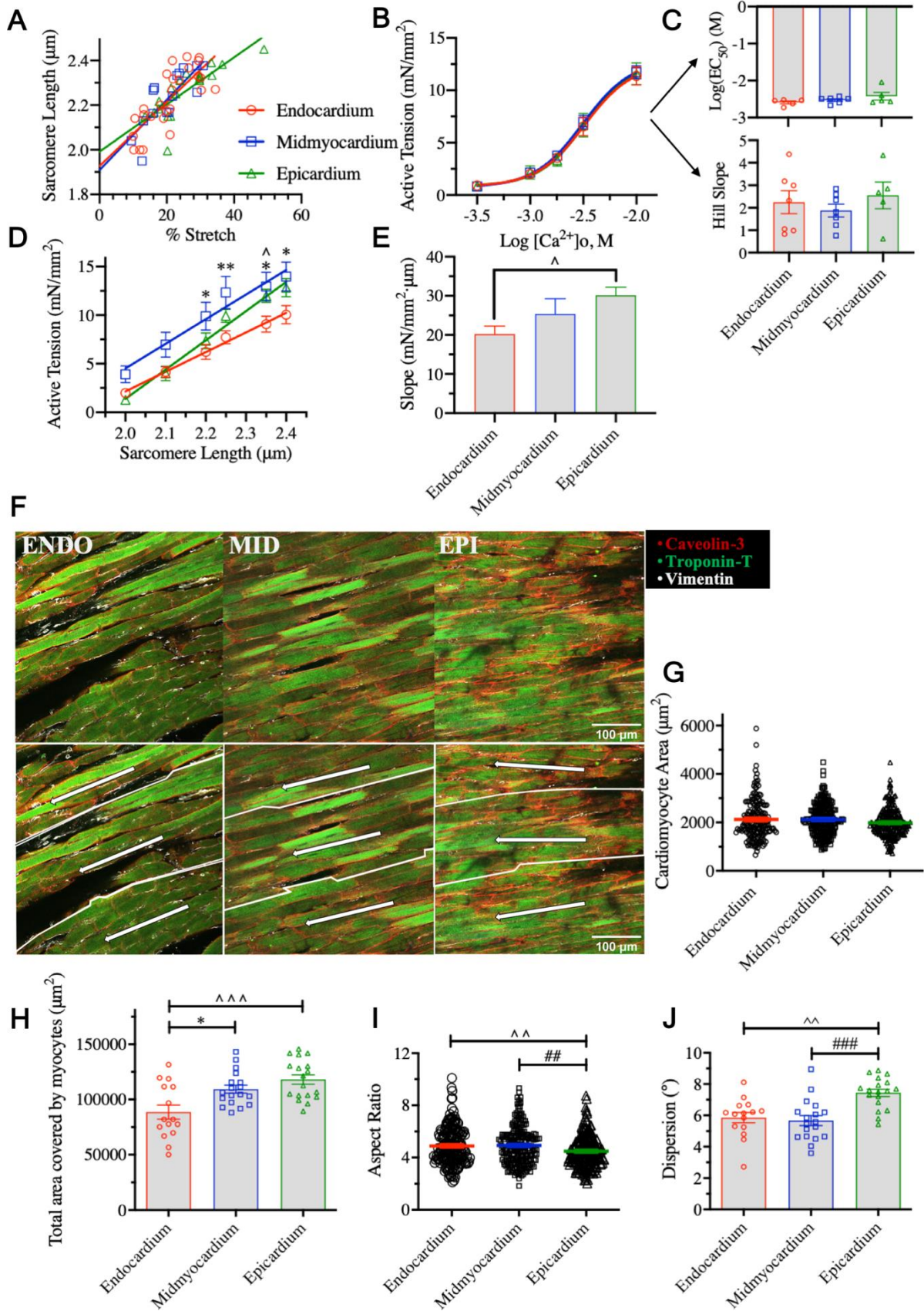
Figure 1: A) Transmural strain-sarcomere length (SL) relationship [N = 6]. B) Concentration-force response curves of cardiac slices from different layers to the external Ca^{2+} concentration ($[Ca^{2+}]o$) [N = 8, N = 7, N = 6]. All force-Ca^{2+} experiments

164 were conducted at 2.1 μm SL. C-Top) Transmural calcium sensitivity as measured
165 by the $\log(EC_{50})$ [N = 5, N = 6, N = 5]. The variable slope concentration-response
166 model fitted did not yield an EC_{50} for three endocardial, one midmyocardial, and one
167 epicardial data sets. C-Bottom) Hill coefficients of the concentration-response
168 curves of each cardiac layer [N = 7, N = 7, N = 5]. The variable slope concentration-
169 response model fitted yielded an ambiguous slope for one endocardial, and one epi-
170 cardial data set. D) Active tension-SL relationship for cardiac slices from different
171 layers of the wall [N = 7, N = 5, N = 7]. E) Slopes of linear regression lines fit to the
172 active tension-SL relationship [N = 7, N = 5, N = 7]. F) Representative confocal im-
173 ages of cardiomyocyte area, density, morphology, and direction. Each image in the
174 bottom panel has been separated into three regions and the major direction of cardio-
175 myocyte orientation drawn with an arrow. The greater the angle between the arrows
176 suggests the greater the variability in cardiomyocyte orientation. G) Cardiomyocyte
177 area [N = 180/5, N = 216/6, N = 216/6]. H) Total myocyte area coverage (myocyte
178 area × number of cardiomyocytes) [N = 15/5, N = 18/6, N = 18/6]. I) Cardiomyocyte
179 aspect ratio [N = 180/5, N = 216/6, N = 216/6]. J) Cardiomyocyte dispersion [N =
180 15/5, N = 18/6, N = 18/6]. All analysis was done blinded. *: midmyocardium vs. en-
181 docardium, ^: epicardium vs. endocardium, #: midmyocardium vs. epicardium. [N =
182 endocardium, midmyocardium, endocardium, and N = images/biological replicates].
183
184 Cardiomyocyte area, which has been reported to be higher in isolated rat endocar-
185 dial than epicardial myocytes[10], was quantified (Fig. 1F-G). Although no differ-
186 ences were found in individual myocyte area, total myocyte coverage of the tissue
187 (myocyte area × number of myocytes) was significantly higher in both midmyocar-
188 dium and epicardium compared to endocardium ($p < 0.05$, and $p < 0.001$ respectively)
189 (Fig. 1H). Cardiomyocyte area is a major determinant of systolic force production
190 and cardiomyocyte density correlates positively with force production in engineered
191 heart tissue[11]. An absolute greater myocyte coverage would thus explain the in-
192 creased active tension-SL relationship and steeper force-stretch response of the mid-
193 myocardium and epicardium. However, cardiomyocyte morphology can also impact
194 cardiac contraction with long and thin myocytes at a mechanical disadvantage when
195 generating force compared to shorter and thicker cells[12]. The cardiomyocyte as-
196 pect ratio (length:width) was significantly lower in epicardial cells compared to both
197 midmyocardium and endocardium (Fig. 1I, $p < 0.01$).
198 Despite the lower aspect ratio, the force-stretch experiments showed that midmyo-
199 cardium produces a higher active tension compared to the endocardium more con-
200 sistently than the epicardium, and does so at a lower SL. We hypothesized that car-
201 diomyocyte orientation could account for this. Cardiomyocyte dispersion, a measure
202 of the standard deviation of a Gaussian curve fitted to the different angulations of
203 structures (i.e. cardiomyocytes) in an image from the main axis of direction was
204 quantified. Dispersion was significantly higher in the epicardium compared to endo-
205 cardium and midmyocardium, suggesting greater cardiomyocyte orientation variabil-
206 ity (Fig. 1J, $p < 0.01$ and $p < 0.001$ respectively). As myocyte misalignment can reduce

207 force development[13], higher cardiomyocyte disorientation may offset force pro-
208 duction in the epicardium despite the lower aspect ratio and explain why the mid-
209 myocardium tends to develop marginally higher active tension than the epicardium
210 when compared to the endocardium (Fig. 1D-E).
211   The sarcomeric apparatus could also underlie transmural differences in active ten-
212 sion. As such, we performed total sarcomeric protein content and phosphoprotein
213 status quantification using Sypro Ruby and ProQ Diamond staining. However, our
214 results showed no significant differences across the wall despite a gradient tendency
215 of certain proteins (Fig. 2A-D). Comparable transmural uniformity of sarcomeric
216 proteins has been reported in the non-failing human heart[2] and rats of similar age
217 by others[14].
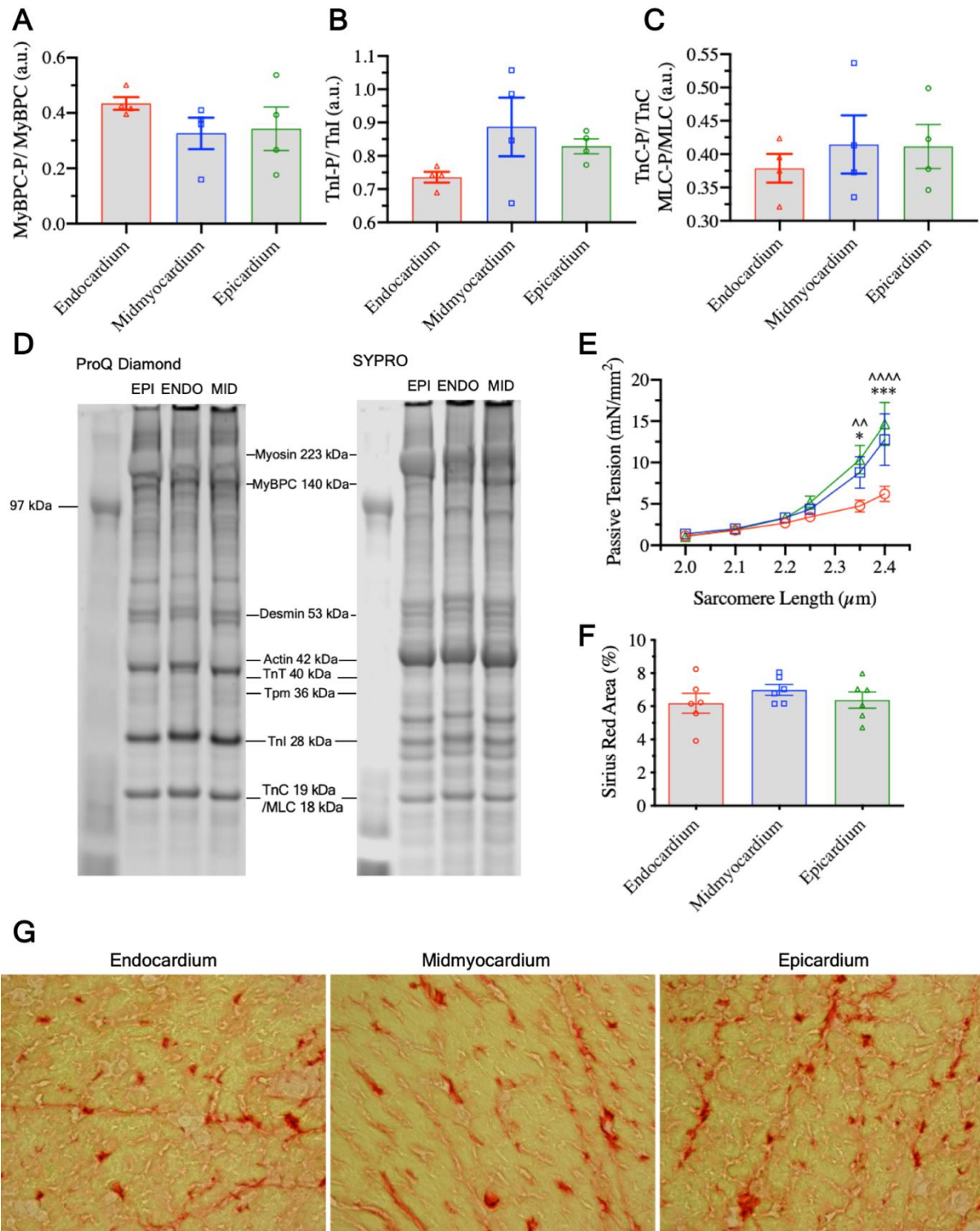
Figure 2: A-C) Ratio of phosphorylated myosin binding protein C, troponin I, and troponin C & myosin light chain to unphosphorylated counterpart respectively [N = 4]. D) Bands from total sarcomeric content (right) and phosphoproteins (left) separated by molecular weight. E) Passive tension-SL relationship for cardiac slices from different layers of the wall [N = 7, N = 5, N = 7]. F) % Area covered by Sirius red staining from transverse cryosections [N = 6]. G) Representative brightfield images of Sirius red staining.*: midmyocardium vs. endocardium, ^: epicardium vs. endocardium. [N = endocardium, midmyocardium, endocardium].

227

Passive tension was significantly lower in the endocardium compared to midmyo-
cardium and epicardium at 2.35 μm and 2.40 μm SL (Fig. 2E, p<0.001 and p<0.0001
at SL of 2.40 μm). In intact isolated cardiomyocytes, passive tension increases more
in the endocardium than epicardium with SL[3]. Data from skinned samples simi-
larly show a stiffer endocardium at high SLs[4], although others have reported no
differences between the two[2][5] nor between the midmyocardium and the other
layers[2]. Our slice data show that intact endocardial layers are less stiff.

Passive tension is particularly important during the refilling phase of the cardiac
cycle. Reconstruction of *in vivo* transmural SL gradients using radiopaque beads and
biplane cineradiography demonstrate that the endocardium operates at a higher and
narrower SL range than the mid- and epicardium, that can reach 2.4 μm length,
where our significant differences arise, prior to ejection[9]. Likewise, the loading
cycle of the isolated arrested heart shows clear transmural deformations (i.e. normal
strains – longitudinal, radial, and circumferential – increase from epicardium to en-
docardium)[15]. The consequences of a) transmural strain gradients, but b) uniform
SL-stretch relationships (Fig. 1A) in the presence of a more compliant endocardium
(Fig. 2E) is a greater deformation of the inner myocardium enabling it to attain a
higher SL. Under this conceptual framework, lower compliance of outer layers
would similarly facilitate their operation at lower SLs while averting excessive en-
docardial diastolic strain, in effect acting as 'guardian' layers.

These conclusions are important not only for diastole but also active cardiac con-
traction. Transmurally non-uniform SLs would position the endocardium further up
and to the right of the Frank-Starling curve and the outer layers further down and to
the left. Intrinsic differences in contractility (Fig. 1A-B), largely attributed here to
structural heterogeneity and total myocyte coverage (Fig. 1G-J), may thus be offset,
homogenizing force production and ventricular pumping efficiency[1]. In support of
this, cardiomyocytes with low aspect ratio develop the highest systolic work in stiff
environments whereas those with higher aspect ratio fare better in less stiff environ-
ments[16], which is in agreement with our functional and structural data.

To uncover the structural factors involved in differential passive tension we per-
formed transverse sectioning of tissue followed by picrosirius red staining. We
found no significant differences in total collagen content between layers (Fig. 2F-G).
Although collagen is a known determinant of passive myocardial mechanics, stiff-
ness is dominated by titin content and isoform composition. In the adult rat, titin, a
giant molecular sarcomeric protein, exists either as larger compliant N2BA or
smaller stiffer N2B isoform. Although we were unable to quantify this, others have
reported extensively that in healthy canine and pig hearts, the N2BA:N2B ratio
shows a transmural gradient highest in the subendocardium[17], consistent with our
mechanical data. Transmural heterogeneity in cross-bridge cycling could also under-
lie the observed differences. Testing this aspect would be insightful and will be part
of future investigations.

A number of limitations are discussed. First, myocardial slices generate stress and
respond to strain across a 2D-plane. This is in contrast to the *in vivo* 3D operation of

271 the heart, where pressure is generated corresponded with distinct changes in volume.
272 Additionally, fiber alignment is known to rotate across the 3D ventricular wall, in
273 contrast to the uniaxial plain of examination in slices. As slices from adjacent layers
274 (1st and 2nd slice & 5th and 6th slice) were collapsed together for data analysis, trans-
275 mural differences may have been underestimated. Another limitation is the use of
276 muscle length control for isometric measurements, which may introduce experi-
277 mental error due to damaged end-compliance[18]. However, the tension-SL relation-
278 ship with muscle length has been suggested to be the same as that of SL control[19].
279 Our data supports that functional differences in transmural mechanics are dominated
280 by structural heterogeneity and not sarcomeric protein content or phosphorylation
281 status. Transmural gradients in myosin light chain phosphorylation have been re-
282 ported [20] and suggested to explain the pattern of active mechanical contraction,
283 which is dominated by the outer layers. However, our results like those of others did
284 not show the presence of such spatial gradients[21].
285   In conclusion, we show for the first time that in intact tissue, intrinsic differences
286 exist in myocardial active and passive mechanics that are primarily governed by
287 structural transmural heterogeneity. *In vivo*, operation of cardiac layers at different
288 SLs has been shown and our findings provide a physiological explanation for this;
289 differences in operating SL seem to be balanced out by differences in the intrinsic
290 mechanical properties.

4. Supplementary Material

4.1. Myocardial Slice Preparation

All animal experiments were conducted in accordance with institutional and national regulations and were approved by Imperial College London, under license by the UK Home Office, United Kingdom Animals (Scientific Procedures) Act 1986.

Myocardial slices were prepared using the protocol previously detailed by Watson et al.[7]. Adult Sprague-Dawley rats (aged 11-15 weeks and 370-450g weight) were sacrificed under anaesthesia (4% isoflurane at 4 L/min oxygen), their heart explanted and placed in 50 ml of heparinized (1000IU/ml) modified Tyrode solution (30.0 mM 2, 3-Butanedione Monoxime, 140.0 mM NaCl, 9.0 mM KCl, 10 mM Glucose, 10.0 mM HEPES, 1.0 mM Magnesium Chloride, 1.0 mM Calcium Chloride; pH 7.40) at 37°C and shortly thereafter at 4°C heparinized modified Tyrode solution. The left ventricle was isolated by removing the lungs and other extra-cardiac structures using a surgical blade and dissecting away the atria and right ventricle. It was then opened up, flattened and the epicardial side glued (Histoacryl®, Braun, Germany) onto a layer of agarose (4% agar) on a specimen holder. The specimen holder was mounted to the tissue bath of a high precision vibrating microtome (7000 smz2, Campden Instruments Ltd., UK) previously filled with oxygenated 4°C modified Tyrode solution.

Before slicing, the vibratome was fitted with a ceramic blade, calibrated to a Z-axis error <1.0 μm and the blade adjusted to have an amplitude of 2 mm, vibration frequency of 80 Hz and advance speed of 0.03 mm/s. These settings were chosen to produce highly viable 300 μm myocardial slices. Each slice generated was examined under light microscopy to determine myocardial fiber orientation. One section with parallel fiber orientation and from the mid-region of each slice was selected and cut into a rectangular sample. The latter was important to minimize apico-basal differences which could confound the results. The length and width of the slice were measured using calipers and recorded for normalization of force to the slice cross-sectional area. For slices used in the contractility, laser diffraction experiments as well as for fixation, custom-designed 3D-printed Polylactic acid (PLA) holders were attached to both ends of the sample perpendicular to the fiber orientation using surgical glue. These were used to manipulate and mount the slice to the force-transducer, laser diffraction, or tissue fixation set-ups.

4.2. Laser Diffraction Experiments

Myocardial slices were mounted on custom-made stainless-steel stretcher using the 3D printed holders. The stretcher was positioned into a glass dish, filled with modified Tyrode's solution at room temperature. A high powered HeNe laser (Lasos, Germany) was positioned 2cm vertically above the slice. The laser was turned on and as it passed through the slice, it diffracted into bands based on the amount of tissue stretch. A camera (Logitech C920 HD) was used to analyze the diffraction profiles in real-time using the plot-profile functionality of ImageJ (National Institute of Health, USA). Each slice was progressively stretched (from slack length) to three

334 different muscle lengths, and the data were used to determine the % stretch-sarco-
335 mere length (SL) relationship. To account for SL inhomogeneity across the tissue,
336 the laser was directed at three different regions of the myocardial slice at each mus-
337 cle length, the SL determined, and then averaged for each stretch.
338   A linear regression model was fit to the % stretch-SL relationship for slices from
339 each cardiac layer. Given a known slice slack length and the linear relationship be-
340 tween stretch and SL, the muscle length correspondent with a desired SL could be
341 calculated. This was subsequently used for fine manipulation of strain in force-cal-
342 cium and Frank-Starling experiments.
343

344 4.3. Force-Calcium Experiments
345   Normal Tyrode's solutions (140.0 mM NaCl, 4.5 mM KCl, 10 mM Glucose, 10.0
346 mM HEPES, 1.0 mM Magnesium Chloride; pH 7.40) with calcium concentrations of
347 0.316 mM ($10^{-3.5}$ M), 1 mM (10^{-3} M), 1.8 mM ($10^{-2.7}$ M), 3.16 mM ($10^{-2.5}$ M), 10 mM
348 ($10^{-2.0}$ M) were prepared.
349   Myocardial slices were moved into an organ bath chamber and mounted on an iso-
350 metric strain gauge (F30 Harvard Apparatus, USA) using the PLA holders. The or-
351 gan bath contained oxygenated 1.8 mM Tyrode's solution at 25°C (starting tempera-
352 ture). Electrical stimulation was initiated, and the temperature of the solution slowly
353 raised until 36 ± 0.5°C. Slices were stretched to a SL of 2.1 μm using muscle length
354 as a surrogate. A micromanipulator and video camera connected to and calibrated
355 with the ImageJ software (National Institute of Health, USA) webcam plugin were
356 used for real-time measurements of muscle-length.
357   Slices were stimulated at 1 Hz, 20-30V amplitude and 10-20 ms width biphasic
358 pulses and data was acquired using AxoScope software (Molecular Devices, USA).
359 After one minute of steady state force production was achieved, perfusion of the cur-
360 rent solution was replaced with a randomly chosen Tyrode's solution containing an
361 unused calcium concentration. This process was repeated until measurements from
362 all calcium concentrations were obtained. At the end, slices were again assessed at
363 1.8 mM Tyrode's solution and if the active tension generated was <60% of the active
364 tension at the first 1.8mM solution, slices were excluded from further analysis.
365   The pClamp software package (Molecular Devices, USA) was used to analyze
366 three force transients generated at the steady state of each calcium concentration
367 (force-calcium) and SL (Frank-Starling – see section 4.4.). The forces generated by
368 the slices were normalized to their cross-sectional area (slice thickness 0.3 mm x
369 slice width).
370   Active tension generated during the force-calcium experiments were plotted
371 against a log scale of Ca^{2+} concentration and a sigmoidal log(agonist) vs. response
372 (variable slope, four parameters) model was fitted according to the equation:

373
$$A = B + C \frac{1}{1 + 10^{((logEc_{50} - \log Ca^{2+})) * H}}$$

374   where A is the active tension, B is the passive tension, C is the maximum force
375   generated, H is the hill coefficient and EC_{50} is the calcium concentration required to
376   reach half maximum active tension.
377

378   4.4. Frank-Starling Experiments (Active and Passive Tension at Different SL)
379   Myocardial slices were mounted onto the isometric strain gauge in the organ bath,
380   containing oxygenated 25°C Tyrode's solution but with $10^{-2.54}$ M Ca^{2+} (EC_{50}) and
381   slowly heated to 36 ± 0.5°C. The slices were progressively stretched to muscle
382   lengths correspondent to SL of 2.0-, 2.10-, 2.20-, 2.25-, 2.35- and 2.40 μm. Slices
383   from different layers were stretched to each SL based on their individual SL-%
384   stretch profiles determined previously from the laser diffraction experiments. All
385   slices were field stimulated at 1 Hz, 20-30V amplitude and 10-20 ms width biphasic
386   pulses using platinum electrodes.
387   A linear regression was fit to the active tension-SL relationship; the gradient of
388   each line was compared to determine the force sensitivity of each cardiac layer to
389   stretch. R^2 values were 0.72, 0.60, and 0.84 for endocardium, midmyocardium, and
390   epicardium respectively.
391
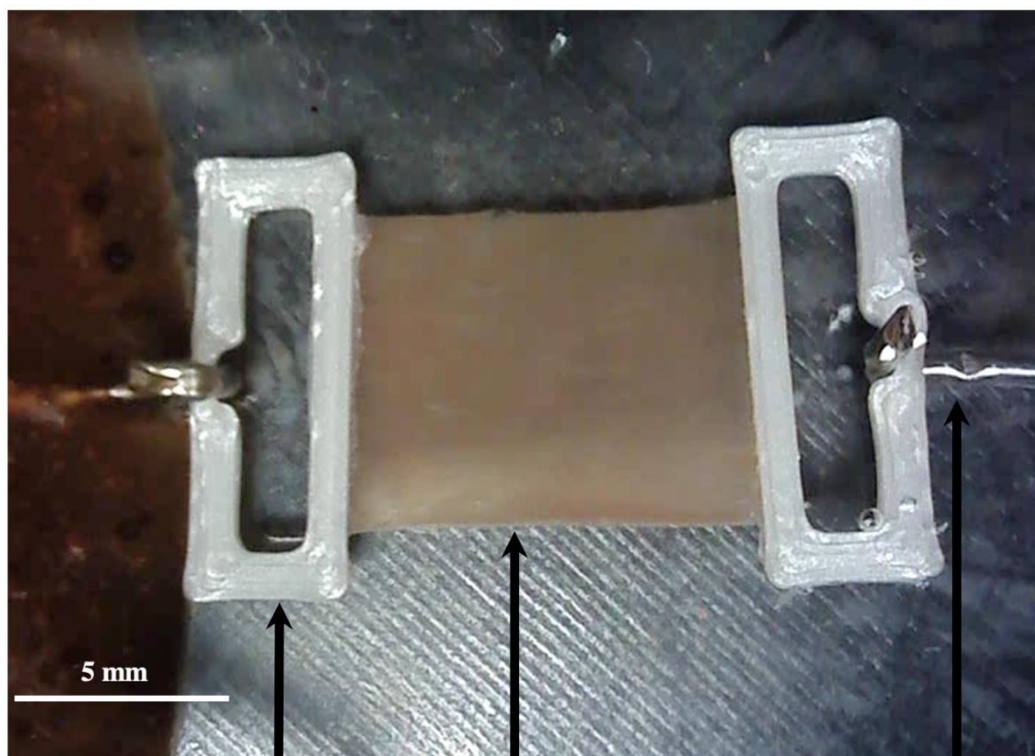
PLA holders   Myocardial Slice   To Strain Gauge Micromanipulator

392
393

Figure 1 Supplementary: Myocardial slice inside the organ bath. 3D-printed PLA holders are attached perpendicular to the direction of myocardial fibers and used to mount the slice on an isometric strain gauge. The slice is stimulated with platinum electrodes (not visible here) at 1Hz and the active and passive tension recorded.

4.5. Immunohistochemical Staining for Confocal Imaging

Cardiac slices were mounted on stretchers, stretched to 2.1 μm SL, and fixed in 4% formaldehyde for 15 minutes at room temperature, washed in phosphate buffered solution (PBS, Sigma), permeabilised and blocked using 1.5% Triton X-100 in 10% FBS, 5% BSA and 10% horse serum for three hours at room temperature on a rocker. Slices were then washed in PBS three times and incubated with their primary antibodies overnight at room temperature on a rocker. After being washed a further three times in PBS, they were incubated with their secondary antibody for 2 hours at room temperature on a rocker, covered with aluminum foil. After a final three washes, the samples were stored at 4ºC in PBS. All stained slices were visualized under confocal microscopy within 1 day of being stained. Myocardial slices were viewed under a confocal microscope (Zeiss LSM-780) and three Z-stack images were taken from each slice at 20x magnification.

Table 1: Antibodies used to stain cardiac slices

Antibody	How it is created	Dilution
Primary Antibodies		
Caveolin 3	Mouse	1:500
Cardiac Troponin T	Rabbit	1:800
Vimentin	Chicken	1:3000
Secondary Antibodies		
Alexa Fluor 488	Donkey, anti-rabbit	1:2000
Alexa Fluor 546	Donkey, anti-mouse	1:2000
Alexa Fluor 647	Goat, anti-chicken	1:2000

Confocal images were analyzed blinded in ImageJ. Caveolin-3 stained the membrane of the cardiomyocytes and allowed identification of the cells and their borders. Length of the cell was defined as the longest axis across a cardiomyocyte and width as the longest line perpendicular to the length axis. Cell area was measured by circumscribing along the cardiomyocyte borders demarked by caveolin-3 staining. Cell density was quantified by counting the number of fully visible cells present in each image. 12 cells were analysed for length:width ratio, and area from each image. Total myocyte area was determined as the product of number of cardiomyocytes × cardiomyocyte area. Vimentin levels were obtained from each image's first four Z-stacks and were normalized using the auto-threshold settings on ImageJ. They were subsequently measured using the pixel quantification tool. Dispersion was calculated using data from all Z-stacks available in the image and measured with the software's directionality analysis tool.

4.6. Sarcomeric Proteins

429   Myofilament fractions were prepared from endocardium, midmyocardium, and epi-
430 cardium as previously described[8]. Myofilament proteins (20 µg per lane) were run
431 on a 4-12 % gradient gel. The gel was then stained with ProQ Diamond according to
432 manufacturer's instructions (Invitrogen). Briefly, the gel was fixed in a 10% acetic
433 acid, 50% methanol solution for one hour. It was then stained with ProQ stain for
434 75 mins and destained with a solution containing 20% acetonitrile, 50 mM sodium
435 acetate, pH 4.00. The resulting gel was imaged using the Typhoon scanner (GE
436 Healthcare) at 580 nm. After imaging, it was stained overnight with Sypro Ruby
437 stain (Invitrogen) and after destain with 10% methanol, 7% acetic acid, it was im-
438 aged using the Typhoon scanner at 619 nm. Band quantification was performed us-
439 ing Image J and the ratio of each phosphorylated protein to total protein was calcu-
440 lated.
441
442 4.7. Picrosirius Red Staining
443   The harvested hearts of six SD rats were blocked in Optimal Cutting Temperature
444 media and stored at -80°C for 24 hours. 7 µm transverse sections were taken by cut-
445 ting the OCT blocks with a cryostat at -23°C and harvested on slides, before being
446 stored at -80°C. To visualize cardiac fibrosis, sections were stained with Picrosirius
447 Red staining kit (ab150681, Abcam). To do that, they were prefixed in Bouin solu-
448 tion for 15 minutes under fume hood at room temperature then washed for 15
449 minutes at room temperature in tap water. Then, sections were stained in Picrosirius
450 red for 1 hour at room temperature under the fume hood. Slides were differentiated
451 in acidified water, twice two dips. Sections were then washed and dehydrated three
452 times in 100% Ethanol before being cleared in Xylene over five minutes. Cover slips
453 were mounted, and imaging was done with brightfield microscope Nikon TE200. 10
454 pictures per area of interest per section were obtained, and two sections were ana-
455 lysed for each animal. The quantification of the red stain was carried out with Im-
456 ageJ. In a first time the original picture was changed to RGB format. Then, a thresh-
457 old previously calibrated in order to cover most of the staining was applied on the
458 RGB picture. After applying the threshold on the picture, the area covered by the
459 stain was measured.
460
461 4.8. Statistical Analysis
462   For comparison of statistical significance between linear regression lines (laser dif-
463 fraction and active tension-SL relationships) analysis of co-variance (ANCOVA)
464 was used. For contractility (active-tension, passive-tension, $logEC_{50}$, Hill slope) and
465 confocal images, the data sets of slices from each layer were compared using one
466 way analysis of variance (ANOVA) with Tukey's post-hoc in Prism8 software
467 (GraphPad, USA). $P<0.05$ was considered statistically significant.

5. Disclosures

Part of this study was featured as an abstract in the European Society of Cardiology Congress, Paris 2019. All authors declare no conflicts of interest, financial or otherwise.

6. Acknowledgements

7. References

[1]   J.M. Cordeiro, L. Greene, C. Heilmann, D. Antzelevitch, C. Antzelevitch, Transmural heterogeneity of calcium activity and mechanical function in the canine left ventricle, Am. J. Physiol. Circ. Physiol. (2004). https://doi.org/10.1152/ajpheart.00748.2003.

[2]   P. Haynes, K.E. Nava, B.A. Lawson, C.S. Chung, M.I. Mitov, S.G. Campbell, A.J. Stromberg, S. Sadayappan, M.R. Bonnell, C.W. Hoopes, K.S. Campbell, Transmural heterogeneity of cellular level power output is reduced in human heart failure, J. Mol. Cell. Cardiol. 72 (2014) 1–8. https://doi.org/10.1016/j.yjmcc.2014.02.008.

[3]   O. Cazorla, J.Y. Le Guennec, E. White, Length - Tension relationships of sub-epicardial and sub-endocardial single ventricular myocytes from rat and ferret hearts, J. Mol. Cell. Cardiol. (2000). https://doi.org/10.1006/jmcc.2000.1115.

[4]   O. Cazorla, S. Szilagyi, J.-Y. Le Guennec, G. Vassort, A. Lacampagne, Transmural stretch-dependent regulation of contractile properties in rat heart and its alteration after myocardial infarction, FASEB J. 19 (2005) 88–90. https://doi.org/10.1096/fj.04-2066fje.

[5]   J. van der Velden, D. Merkus, V. de Beer, N. Hamdani, W.A. Linke, N.M. Boontje, G.J.M. Stienen, D.J. Duncker, Transmural Heterogeneity of Myofilament Function and Sarcomeric Protein Phosphorylation in Remodeled Myocardium of Pigs with a Recent Myocardial Infarction, Front. Physiol. 2 (2011). https://doi.org/10.3389/fphys.2011.00083.

[6]   J.E. Stelzer, H.S. Norman, P.P. Chen, J.R. Patel, R.L. Moss, Transmural variation in myosin heavy chain isoform expression modulates the timing of myocardial force generation in porcine left ventricle, J. Physiol. (2008). https://doi.org/10.1113/jphysiol.2008.160390.

[7]   S.A. Watson, M. Scigliano, I. Bardi, R. Ascione, C.M. Terracciano, F. Perbellini, Preparation of viable adult ventricular myocardial slices from large and small mammals., Nat. Protoc. 12 (2017) 2623–2639. https://doi.org/10.1038/nprot.2017.139.

[8]   M. Papadaki, R.J. Holewinski, S.B. Previs, T.G. Martin, M.J. Stachowski, A. Li, C.A. Blair, C.S. Moravec, J.E. Van Eyk, K.S. Campbell, D.M. Warshaw, J.A. Kirk, Diabetes with heart failure increases methylglyoxal modifications in the sarcomere, which inhibit function, JCI Insight. (2018). https://doi.org/10.1172/jci.insight.121264.

[9]   E.K. Rodriguez, W.C. Hunter, M.J. Royce, M.K. Leppo, A.S. Douglas, H.F. Weisman, A method to reconstruct myocardial sarcomere lengths and orientations at transmural sites in beating canine hearts, Am. J. Physiol. Circ. Physiol. (1992). https://doi.org/10.1152/ajpheart.1992.263.1.h293.

[10] A.M. Gerdes, J.A. Moore, J.M. Hines, P.A. Kirkland, S.P. Bishop, Regional differences in myocyte size in normal rat heart, Anat. Rec. (1986). https://doi.org/10.1002/ar.1092150414.

[11] F. Weinberger, I. Mannhardt, T. Eschenhagen, Engineering Cardiac Muscle Tissue: A Maturing Field of Research, Circ. Res. 120 (2017) 1487–1500. https://doi.org/10.1161/CIRCRESAHA.117.310738.

[12] A.M. Gerdes, J.M. Capasso, Structural remodeling and mechanical dysfunction of cardiac myocytes in heart failure, J. Mol. Cell. Cardiol. (1995). https://doi.org/10.1016/0022-2828(95)90000-4.

[13] M.L. Munro, X. Shen, M. Ward, P.N. Ruygrok, D.J. Crossman, C. Soeller, Highly variable contractile performance correlates with myocyte content in

526   trabeculae from failing human hearts, Sci. Rep. (2018).
527   https://doi.org/10.1038/s41598-018-21199-y.

528 [14]   S.G. Campbell, P. Haynes, W.K. Snapp, K.E. Nava, K.S. Campbell, Altered
529   ventricular torsion and transmural patterns of myocyte relaxation precede
530   heart failure in aging F344 rats, Am. J. Physiol. - Hear. Circ. Physiol. (2013).
531   https://doi.org/10.1152/ajpheart.00797.2012.

532 [15]   J.H. Omens, K.D. May, A.D. McCulloch, Transmural distribution of three-
533   dimensional strain in the isolated arrested canine left ventricle, Am. J. Physiol.
534   - Hear. Circ. Physiol. (1991).
535   https://doi.org/10.1152/ajpheart.1991.261.3.h918.

536 [16]   M.L. McCain, H. Yuan, F.S. Pasqualini, P.H. Campbell, K.K. Parker, Matrix
537   elasticity regulates the optimal cardiac myocyte shape for contractility, Am. J.
538   Physiol. Circ. Physiol. (2014). https://doi.org/10.1152/ajpheart.00799.2013.

539 [17]   S.P. Bell, L. Nyland, M.D. Tischler, M. McNabb, H. Granzier, M.M.
540   LeWinter, Alterations in the determinants of diastolic suction during pacing
541   tachycardia, Circ. Res. (2000). https://doi.org/10.1161/01.RES.87.3.235.

542 [18]   P.P. de Tombe, H.E.D.J. ter Keurs, Cardiac muscle mechanics: Sarcomere
543   length matters, J. Mol. Cell. Cardiol. 91 (2016) 148–150.
544   https://doi.org/10.1016/j.yjmcc.2015.12.006.

545 [19]   H.E.D.J. Ter Keurs, W.H. Rijnsburger, R. Van Heuningen, M.J. Nagelsmit,
546   Tension development and sarcomere length in rat cardiac trabeculae. Evidence
547   of length-dependent activation, Circ. Res. (1980).
548   https://doi.org/10.1161/01.RES.46.5.703.

549 [20]   J.S. Davis, S. Hassanzadeh, S. Winitsky, H. Lin, C. Satorius, R. Vemuri, A.H.
550   Aletras, H. Wen, N.D. Epstein, The overall pattern of cardiac contraction
551   depends on a spatial gradient of myosin regulatory light chain
552   phosphorylation, Cell. (2001). https://doi.org/10.1016/S0092-8674(01)00586-
553   4.

554 [21]   J. Huang, J.M. Shelton, J.A. Richardson, K.E. Kamm, J.T. Stull, Myosin
555   regulatory light chain phosphorylation attenuates cardiac hypertrophy, J. Biol.
556   Chem. 283 (2008) 19748–19756. https://doi.org/10.1074/jbc.M802605200.

557